Macromolecules

pubs.acs.org/Macromolecules
Article

Effect of Pressure on the Micellar Structure of PMMA-*b*-PNIPAM Diblock Copolymers in Aqueous Solution

Pablo A. Alvarez Herrera, Geethu P. Meledam, Bart-Jan Niebuur, Yamen Taji, Leonardo Chiappisi, Cristiane Henschel, André Laschewsky, Alfons Schulte,* and Christine M. Papadakis*

Cite This: *Macromolecules* 2024, 57, 10263−10274

ABSTRACT: The phase behavior as well as the pressure- and temperature-dependence of the micellar structure of the thermoresponsive amphiphilic diblock copolymer $PMMA_{21}$-*b*-$PNIPAM_{283}$ in D_2O are investigated. The coexistence line of $PMMA_{21}$-*b*-$PNIPAM_{283}$ in D_2O in the temperature−pressure frame is shifted to lower in temperature and pressure compared to PNIPAM homopolymers in D_2O. High-pressure small-angle neutron scattering (SANS) provides insights into the structure and aggregation behavior of the micelles both in the one-phase and the two-phase regions. In the one-phase region, pressure does not noticeably alter the core−shell structure of the micelles. Upon heating the solution at atmospheric pressure into the two-phase region, the micellar shell strongly dehydrates and shrinks. Conversely, the micellar shell remains hydrated when the coexistence line is crossed either by heating at 35 and 75 MPa, or by increasing the pressure at 31.8 °C. Moreover, along both pathways, the aggregates in the two-phase region are significantly larger than at atmospheric pressure.

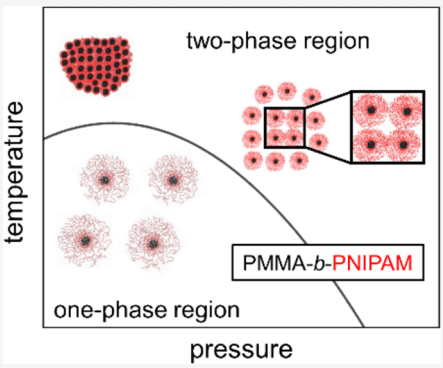

1. INTRODUCTION

Self-assembly is a ubiquitous phenomenon in soft matter systems, such as colloids, liquid crystals, surfactants, and amphiphilic diblock copolymers.[1−6] Self-assembly arises from the intrinsic tendency of these materials to spontaneously organize into well-defined structures driven by various factors, such as temperature and pressure. These parameters significantly influence the spatial arrangements and morphologies of self-assembled structures, governing their stability, dynamics, and functional properties. In the past years, the effect of pressure on thermoresponsive polymer solutions has attracted considerable attention. Thermoresponsive polymers are a subclass of stimuli-responsive polymers that react to small temperature changes by reversible changes in their solvation state.[7] They are important for a wide range of applications, such as drug delivery systems, tissue engineering, sensors, separation membranes, smart textiles, and catalysis.[8−11] Poly(*N*-isopropylacrylamide) (PNIPAM) is a well-known example, featuring lower critical solution temperature (LCST) behavior in aqueous solution with a sharp and reversible coil-to-globule transition at the cloud point T_{cp} of 30−32 °C in a wide range of molar masses and concentrations.[12,13] Below T_{cp}, PNIPAM is water-soluble with a random-coil conformation, which was attributed to the formation of sequential hydrogen bonds between the amide groups of PNIPAM and water molecules.[14,15] Upon heating through T_{cp}, due to the increase of the entropic penalty arising from hydrophobic hydration, the PNIPAM chains dehydrate and collapse, resulting in large, compact aggregates, named mesoglobules.[16−19] Applying pressure alters the hydration behavior, which, for aqueous PNIPAM solutions, has proven to give new insights into the phenomena observed at the LCST transition.[20] For PNIPAM homopolymers in aqueous solution, the T_{cp}-values lie on a line that features a convex upward shape in the temperature−pressure frame.[21−24] The deuteration of the solvent only causes a minor shift in the temperature of the phase boundary, and no substantial change in the transition behavior is observed.[21,25] An important difference between the phase separation induced by increasing the pressure rather than temperature is that, for the former, the number of hydrogen bonds between the amide group of PNIPAM and water increases, and the PNIPAM chains are more hydrated.[26−28] The hydrogen bonds between the hydrophobic alkyl groups and water are strengthened and the dehydration of the PNIPAM chains occurs over a broader temperature range.[27,29] Moreover, the polymer maintains a swollen and hydrated conformation, even in the two-phase region.[26,27,29]

Received: July 9, 2024
Revised: August 28, 2024
Accepted: October 2, 2024
Published: October 16, 2024

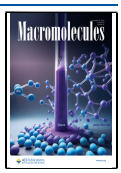

https://doi.org/10.1021/acs.macromol.4c01591
Macromolecules 2024, 57, 10263−10274

In the present study, we address these effects in a more complex, self-assembled system, namely a micellar solution. It is well-known that amphiphilic diblock copolymers with a short hydrophobic and a long hydrophilic block form spherical core−shell micelles with the hydrophobic block forming the core and the hydrophilic block the shell.[6,30−33] Pressure changes offer an alternative to temperature changes for controlling the structure of block copolymer materials, which may alter their macroscopic properties. Here, we investigate the influence of pressure on a micellar solution of a diblock copolymer comprising a short hydrophobic poly(methyl methacrylate) (PMMA) block and a long thermoresponsive PNIPAM block, namely a $PMMA_{21}$-*b*-$PNIPAM_{283}$ solution in D_2O. Ambient pressure studies on this system have shown that, below T_{cp}, spherical micelles with a dehydrated PMMA core and a water-swollen PNIPAM shell are formed, with the latter exhibiting a radially decaying gradient of PNIPAM concentration.[34] At temperatures just above T_{cp}, the micellar PMMA core shrinks slightly, while the PNIPAM shell undergoes strong dehydration and contraction. Small fractal clusters are formed by the micelles, that grow into large compact aggregates upon further temperature increase.[34] Similar behavior was observed when, e.g., polystyrene was used as a hydrophobic block.[35−40] However, these micelles may be kinetically frozen, which is not the case for the $PMMA_{21}$-*b*-$PNIPAM_{283}$.[41]

An intriguing question is how the structures of such micellar solutions react to high pressure. Small-angle neutron scattering (SANS) is the method of choice to probe the structural evolution of micellar solutions from $PMMA_{21}$-*b*-$PNIPAM_{283}$ with pressure because this method gives information not only about the size of the micelles, but also about their inner structure, their correlation and their aggregation.[42] Hence, after having determined the pressure-dependent cloud-point temperatures T_{cp}, we use SANS to investigate the temperature-dependent changes across the respective T_{cp} as well as the pressure-dependent changes at fixed temperature. This allows us to investigate the effect of pressure on the micellar structure as well as on the dehydration and aggregation behavior at low and high pressure.

While we are not aware of investigations of the effect of pressure on micellar solutions from diblock copolymers with a hydrophobic core and a thermoresponsive shell, such as PMMA-*b*-PNIPAM, a few studies have addressed (non-responsive) amphiphilic diblock copolymers in selective organic solvents[43,44] or in aqueous solution.[45,46] These studies focused primarily on the effect of pressure on the transitions between various disordered or ordered phases in rather concentrated block copolymer solutions. Few studies addressed doubly thermoresponsive diblock copolymers in which one block features LCST behavior and the other one upper critical solution temperature behavior.[47] In other studies, doubly thermoresponsive diblock copolymers in aqueous solution were investigated.[48−50] Spherical micelles formed by diblock copolymers comprising a poly(2-ethoxyethoxyethyl vinyl ether) (pEOEOVE) and a poly(2-hydroxyethyl vinyl ether) (pHOVE) were observed to transition into a body-centered cubic (bcc) structure for temperatures between the T_{cp}'s of pEOEOVE and pHOVE. If was found that pressure weakens the selective hydration of pHOVE, which leads to a higher water content in the micellar core formed by pEOEOVE.[50] We note that these polymers show the classical type I LCST behavior, whereas the here studied PNIPAM − even though being considered to be a prototype thermoresponsive polymer−belongs to the class of type II LCST polymers, which is less common.[13]

The manuscript is structured as follows: We determine the phase diagram of a 5 wt % solution of the diblock copolymer $PMMA_{21}$-*b*-$PNIPAM_{283}$ in D_2O in the pressure−temperature frame by turbidimetry. Then, we characterize the micellar structures and aggregation behavior in heating scans across the coexistence line by SANS measurements at pressures ranging from 0.1 MPa (atmospheric pressure) to 75 MPa, i.e., across the maximum of the coexistence line. Additionally, the micellar structure of $PMMA_{21}$-*b*-$PNIPAM_{283}$ is characterized in an isothermal pressure scan at 31.8 °C from the one-phase to the two-phase region.

2. EXPERIMENTAL SECTION

2.1. Materials. The diblock copolymer $PMMA_{21}$-*b*-$PNIPAM_{283}$ was synthesized by reversible addition−fragmentation chain transfer (RAFT) polymerization as described previously.[34] The number-average molar mass M_n of the polymer is 35,000 g mol^{-1} and the dispersity $Đ$ is 1.39. For the turbidimetry and SANS measurements, the polymer was dissolved in D_2O (Deutero GmbH, purity 99.95%, Kastellaun, Germany) at a polymer concentration of 50 g L^{-1}. Afterward, the solution was shaken for 48 h at room temperature.

2.2. Methods. *2.2.1. Turbidimetry.* Turbidimetry measurements were performed to determine the cloud points in dependence on pressure. The experimental setup consists of a custom-made copper−beryllium high-pressure sample cell, which can withstand pressures up to 400 MPa, placed between a 10 mW HeNe laser (λ = 632.8 nm) and a photodiode detector (Thorlabs GmbH, Germany), as described elsewhere.[23] Inside the cell, a Viton O-ring is placed between two sapphire windows to separate the sample from the pressurizing medium (water). The light path through the sample was 1 mm. A hand-operated pressure generator (SITEC, Maur, Switzerland) was employed to pressurize the solution. The temperature of the cell was controlled by a Julabo F12 thermostat (Julabo GmbH, Seelbach, Germany). The transmitted light intensity was measured as a function of the temperature at pressures, between atmospheric pressure and 200 MPa. At this, the temperature was increased at a heating rate of 0.5 K min^{-1}. The measured transmitted intensity was normalized to its maximum value in each temperature scan. The cloud point was determined as the temperature at which the normalized transmitted intensity starts to decrease.

2.2.2. Small-Angle Neutron Scattering (SANS). SANS measurements were carried out at instrument D11 at the Institut Laue-Langevin (ILL), Grenoble, France.[51] The incident neutron beam had a wavelength λ = 6 Å with a spread $\Delta\lambda/\lambda$ = 0.09. The momentum transfer q is $q = 4\pi \sin(\theta/2)/\lambda$, where θ is the scattering angle. Sample-to-detector distances (SDDs) of 1.5, 8.0, and 34 m were used, resulting in a q-range of q = 0.013−4.3 nm^{-1}. The sample was mounted in a copper−beryllium cell, which can withstand pressures up to 350 MPa.[52] Measuring times were 3 min for SDDs of 1.5 and 8.0 m, and 15 min for 34 m. The scattering intensity of the empty pressure cell and the dark current measured using boron carbide were subtracted from the data. H_2O was utilized to calibrate the detector sensitivity and to bring the data to absolute scale. These operations were carried out using the LAMP software.[53]

2.2.3. Modeling of the SANS Data. Structural models were employed to analyze the SANS curves depending on the position in the temperature−pressure frame. In the one-phase region, the SANS curves were analyzed by a model that consists of four contributions

$$I(q) = I_P(q) + I_0 I_{exp}(q) S_{SHS}(q) + I_{OZ}(q) + I_{bkg} \quad (1)$$

where $I_P(q)$ is the Porod term that describes the scattering of large aggregates,[54] which dominates at low q-values, $I_{exp}(q)$ is the form factor of polydisperse core−shell spheres with the polymer concentration in the shell featuring an exponential decay along the

https://doi.org/10.1021/acs.macromol.4c01591
Macromolecules 2024, 57, 10263−10274

radial coordinate,[55] $S_{SHS}(q)$ is the sticky hard-sphere structure factor,[56,57] which is used to describe the spatial correlation between the micelles, I_0 is the scaling constant of the form factor, $I_{OZ}(q)$ is the Ornstein−Zernike structure factor that describes the spatial correlation of concentration fluctuations inside the micellar shell,[58] and I_{bkg} is a constant background, which describes the incoherent scattering. For the detailed equations, see the Supporting Information (eqs S1−S22).

$I_P(q)$ features the Porod exponent m, which gives information about the roughness of the surface of the aggregates: $m = 4$ is obtained for smooth surfaces, $m < 4$ is obtained for rough surfaces, and $m > 4$ is obtained when the aggregates feature a concentration gradient perpendicular to their surface.[59,60] $I_{exp}(q)$ contains the radius of the micellar core, R_c, and the thickness of the micellar shell, ΔR, as free parameters. Thus, the micellar radius is determined as $R_m = R_c + \Delta R$. The polydispersity of R_c was modeled by the Schulz-Zimm distribution.[61] The scattering length density (SLD) in the shell $\eta_{exp,sh}(r)$, was modeled by an exponential function along the radial direction r. $\eta_{exp,sh}(r)$ depends on the following parameters: the decay length of the SLD in the shell α, which gives insights into the penetration of the solvent inward the micellar shell, and the solvent fractions at R_c and at $R_c + \Delta R$, which are Φ_{in} and Φ_{out}, respectively. $S_{SHS}(q)$ features a short-ranged attractive interaction, besides the hard-sphere repulsion, and gives the hard-sphere radius R_{HS}, namely, the half of the average distance between the centers of the correlated micelles, the hard-sphere volume fraction f_s, i.e., the fraction of the overall volume which is occupied by the hard-spheres (stiff regions of the micelles which do not overlap), and the stickiness parameter τ, which characterizes the depth of the attractive potential. The second virial coefficient b_2, which indicates the sign and magnitude of the interaction between the hard-spheres, is related to τ by[62] $b_2 = 1 - (4\tau)^{-1}$. The interaction is repulsive for $b_2 > 0$, while it is attractive for $b_2 < 0$. Finally, $I_{OZ}(q)$ features the correlation length of the concentration fluctuations in the micellar shell ξ.

At atmospheric pressure, the SANS curves in the two-phase region were fitted by the following model

$$I(q) = I_{GP}(q) + I_{OZ}(q) + I_{bkg} \quad (2)$$

where $I_{GP}(q)$ is the Guinier-Porod form factor describing the scattering from the aggregates formed by the collapsed micelles.[60] $I_{GP}(q)$ gives the radius of gyration of the aggregates, R_g, and the Porod exponent m.

At pressures higher than 0.1 MPa, the SANS curves in the two-phase region were modeled by

$$I(q) = I_P(q) + I_0 I_{CS}(q) S_{HS}(q) + I_{OZ}(q) + I_{bkg} \quad (3)$$

where $I_p(q)$ is the Porod term, $I_{CS}(q)$ is the form factor of monodisperse core−shell spheres with a constant SLD in the shell,[63] which has the radius of the micellar core R_c, the thickness of the micellar shell ΔR, and the fraction of solvent inside the shell Φ, as free parameters. I_0 is the scaling constant of the form factor. $S_{HS}(q)$ is the Percus−Yevick hard-sphere structure factor,[64] which contains the hard-sphere radius R_{HS}, and the hard-sphere volume fraction, f_s.

The SANS profiles were fitted using the SASFit software.[65] The instrumental smearing was considered by including the resolution function during model fitting.

3. RESULTS AND DISCUSSION

In this section, we first present the phase diagram of a 50 g L^{-1} solution of $PMMA_{21}$-*b*-$PNIPAM_{283}$ in D_2O in the temperature−pressure frame. Then, the characterization of its micellar structure by SANS measurements in dependence on temperature and pressure is presented. Finally, the results are summarized and discussed.

3.1. Determination of the Phase Diagram. Figure 1a shows the normalized light transmission curves at different pressures as a function of the temperature. Most prominent is the continuously increasing shift of the clouding transition to lower temperatures with increasing pressure at pressures above 25 MPa. While the decays of the transmission are sharp at low pressures, they extend over broader temperature ranges, as pressure is increased above 100 MPa. This indicates that, at higher pressure, the formation of aggregates, which scatter the light, occurs more gradually than at low pressures. The phase diagram in the temperature−pressure frame is constructed from the cloud points T_{cp}, identified from the start of the decays (Figure 1b). The T_{cp}-values seem to lie on an ellipse, similar to our previous observations on aqueous solutions of PNIPAM homopolymers.[23,24] However, fitting the cloud points with an ellipse is difficult here, due to the limited range of pressures used in the turbidimetry measurements (0.1−200 MPa), thus covering only a small portion of the ellipse. Therefore, a parabola was used to fit the data points (for the details see section 2 of the SI) and to determine the maximum of the coexistence line (Figure 1b). The maximum of the coexistence line is located at p_{max} = 30.3 MPa and T_{max} = 31.1 °C. Thus, it is shifted to lower pressure and temperature compared to the aqueous solution of the homopolymer PNIPAM in D_2O (p_{max} = 60.0 MPa and T_{max} = 35.9 °C).[23] This indicates that the one-phase region is destabilized by the coupling of PNIPAM to a PMMA block, i.e., the solubility of the PNIPAM chains is reduced. This may be attributed to the limited accessibility of the solvent in the inner part of the micellar shell, implying a partial dehydration of the PNIPAM chains close to the micellar core. This effect was observed before at atmospheric pressure for di- and triblock copolymers having a thermoresponsive block and one or two short polystyrene blocks.[66,67] A similar effect is observed at atmospheric pressure in the present system: T_{cp} of the PMMA-*b*-PNIPAM solution is 29.9 °C (Figure 1a), whereas it was found at 33.6−33.7 °C for a PNIPAM homopolymer in D_2O at a similar polymer concentration (3 wt %).[26]

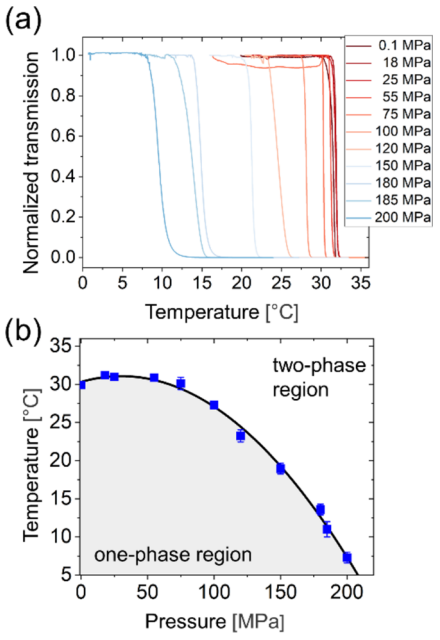

Figure 1. (a) Normalized light transmission of the PMMA-*b*-PNIPAM solution in D_2O (50 g L^{-1} in D_2O) as a function of the temperature, measured during heating scans at the pressures indicated in the graph (b) Resulting cloud points (symbols). The black solid line is the fit of the data by a parabola.

https://doi.org/10.1021/acs.macromol.4c01591
Macromolecules 2024, 57, 10263−10274

3.2. Characterization of the Micellar Structure. To gain insights about the underlying mechanisms of the aggregation process, and the effect of pressure on the micellar structures and their correlations, SANS experiments were performed on the PMMA-*b*-PNIPAM solution in different regions in the temperature−pressure frame.

3.2.1. Overview. Temperature-resolved SANS experiments (temperature scans) across the coexistence line were conducted between 25 and 35 °C at pressures of 0.1 MPa (i.e., atmospheric pressure), 35, and 75 MPa (see the arrows in Figure 2). Additionally, the coexistence line was crossed by

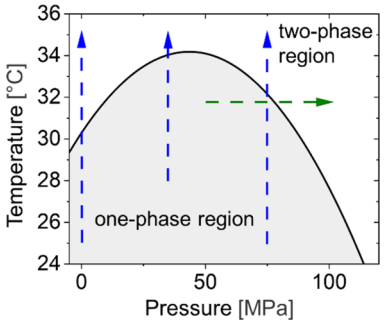

Figure 2. Phase diagram of the PMMA-*b*-PNIPAM solution (50 g L^{-1} in D_2O), as deduced from SANS (solid black line). The temperature scans at 0.1, 35, and 75 MPa are indicated with blue arrows, while the pressure scan at 31.8 °C is indicated with a green arrow.

increasing the pressure (pressure scan) from 50 to 100 MPa at 31.8 °C (Figure 2). The relatively high polymer concentration of 50 g L^{-1} was selected to ensure a high scattering signal in SANS and thus good statistics in the scattering data from this complex system. D_2O was selected as the solvent to obtain a maximum scattering contrast between the polymer and the solvent. Our previous results on similar block copolymers show that there is no qualitative difference in phase behavior and structures with respect to the ones in H_2O.[68,69] We noticed that there was a slight mismatch in the clouds points between the values from turbidimetry and at those temperatures, where strong changes occur in the structural parameters resulting from the analysis of the SANS data (Figure S1 in the SI). This mismatch corresponds to a positive shift of the maximum of the coexistence line (p_{max}, T_{max}) of ca. 12 MPa and ca. 2.5 °C with respect to the position determined by turbidimetry (Figure 1b). This may be due to a difference in temperature calibration between the two setups and to the difference in identification criteria. Therefore, we determined the coexistence line from the SANS parameters by fitting again a parabola (eq S23 in the SI), which serves as a guideline for the interpretation of the results from the SANS experiments. In the following, we discuss first the three temperature scans, then the pressure scan, before we summarize the results.

3.2.2. Temperature Scans at Various Pressures. The SANS curves from the temperature scans at 0.1 and 75 MPa are shown in Figure 3a,b, both unshifted and shifted. The SANS curves at 35 MPa are shown in Figure S2 in the SI. At 0.1 MPa and at 25−30 °C (i.e., below T_{cp}, Figure 3a), the curves feature a weak maximum along with a shoulder at $q \cong 0.2$ nm^{-1}, which shifts toward slightly higher q-values and becomes less pronounced, as the temperature is increased up to 30 °C. We assign these features to the combination of the form and structure factor of individual micelles. A plateau emerges below $q \cong 0.1$ nm^{-1}, whose intensity progressively increases upon heating to 30 °C. Also, a straight decay appears below $q \cong 0.03$ nm^{-1} in this temperature range. This decay points to the presence of large-scale inhomogeneities, as observed previously in a small-angle X-ray experiment (with limited q-range, down to ca. 0.025 nm^{-1}).[34] At 31 °C, the profile features a shoulder at $q \cong 0.05$ nm^{-1} and a plateau at lower q-values. We attribute this change of shape to the transition from the one-phase to the two-phase region. Between 32−35 °C, i.e., above T_{cp}, the shoulder at $q \cong 0.20$ nm^{-1}, which we observed below T_{cp}, i.e., the form factor scattering of single micelles, vanishes. Moreover, the prominent shoulder at $q \cong 0.05$ nm^{-1} observed at 31 °C shifts to lower q-values as temperature increases, indicating the growth of large structures.

At 75 MPa (Figure 3b), the SANS curves feature a shoulder at $q \cong 0.2$ nm^{-1} below T_{cp}. Also, a plateau between 0.03 and 0.1 nm^{-1} is observed at temperatures up to 31 °C. When the temperature is increased further up to T_{cp}, however, a decay is observed in this q-region. Moreover, a straight decay is also present below $q \cong 0.03$ nm^{-1}, but contrary to the 0.1 MPa data, its intensity increases markedly as temperature approaches T_{cp}. Above T_{cp}, on the other hand, the curves display a prominent correlation peak at $q \cong 0.4$ nm^{-1}. The temperature scan at 35 MPa shows similar features below and above T_{cp} (Figure S2 in the SI). However, the peak at 75 MPa is located at a slightly lower q-value than the one at 35 MPa, and the correlation peak at 75 MPa is sharper than the one at 35 MPa, indicating that pressure affects the correlation between the micelles in the two-phase region.

To obtain detailed information about the pressure- and temperature-dependence of the micellar structure and of the aggregation behavior of PMMA-*b*-PNIPAM in D_2O, the SANS curves were fitted with structural models. The lower plots of Figure 3 show the SANS data with their model fits. To carry out the modeling of the SANS curves, three regimes were identified in the temperature−pressure frame: First, in the one-phase region, i.e., below T_{cp}, the SANS data from the three temperature scans can all be described by eq 1. This model suggests that PMMA-*b*-PNIPAM in D_2O self-assembles into spherical core−shell micelles with a homogeneous core and with the polymer concentration in the shell featuring an exponential decay along the radial direction (eqs S2−S8 in the SI). A radially decaying polymer concentration in the micellar shell was previously reported for aqueous solutions of micelle-forming PS-*b*-PNIPAM[38] and the PMMA-*b*-PNIPAM diblock copolymer investigated here,[34] both at atmospheric pressure. Furthermore, a short-range attractive potential, besides the hard-sphere repulsion, is included to model the correlation between the micelles (eqs S10−12 in the SI). The sticky hard-sphere structure factor $S_{SHS}(q)$ was previously employed to analyze SAXS data of this polymer below T_{cp} at atmospheric pressure.[34] The other components of the model are the Porod term (eq S1 in the SI) that is used to describe the scattering from large aggregates, the Ornstein−Zernike structure factor (eq S13 in the SI) that describes the scattering at high q-values due to the concentration fluctuations in the swollen PNIPAM shell, and a constant background. An example is shown in Figure 4a, namely, the full fitting function and its contributions.

At atmospheric pressure and above T_{cp}, only the contributions from large aggregates and the concentration fluctuations inside them are included (eq 2 and Figure 4b). We attribute this to the strong dehydration of the micellar shell and the intermicellar regions and the subsequent loss of

https://doi.org/10.1021/acs.macromol.4c01591
Macromolecules 2024, 57, 10263−10274

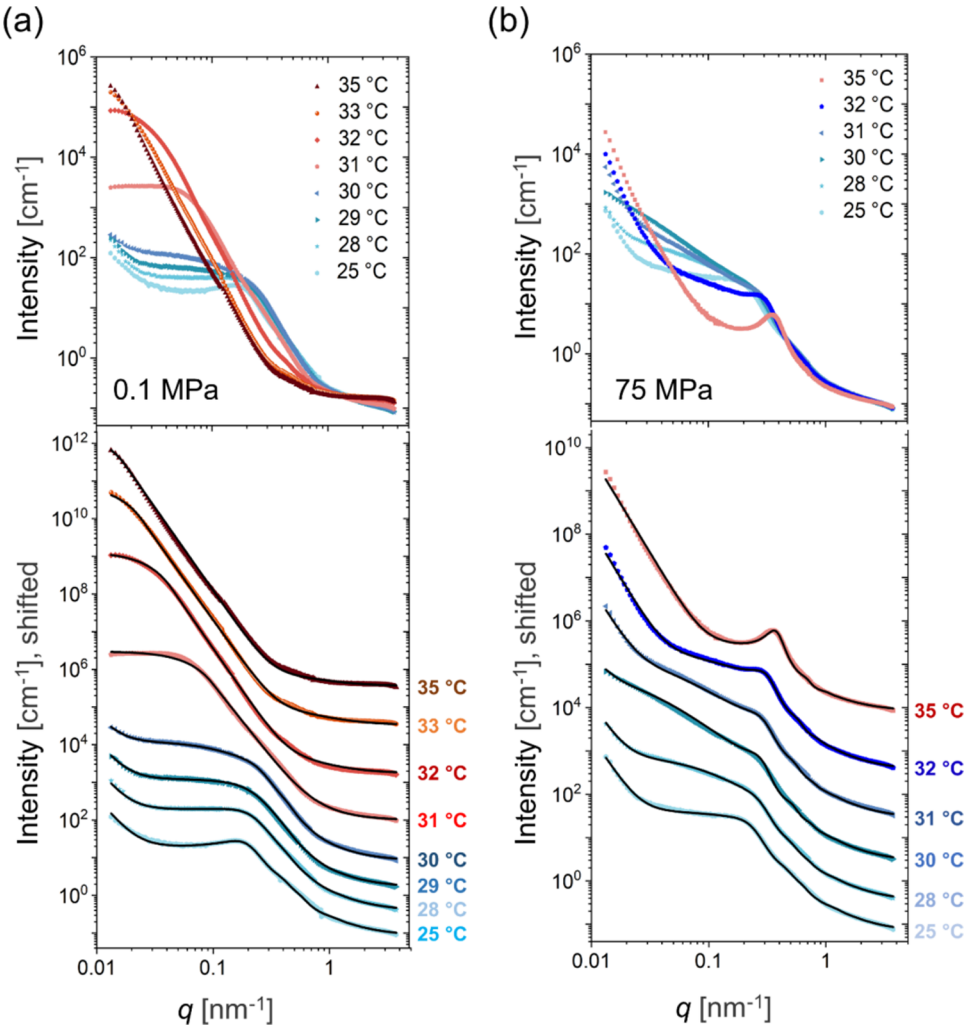

Figure 3. SANS data of the PMMA-*b*-PNIPAM solution (50 g L^{-1} in D_2O) from the temperature scans at (a) 0.1 MPa and (b) 75 MPa. Upper graphs: unshifted data, lower graphs: vertically shifted data (symbols) with model fits (solid black lines). The SANS curves below and above T_{cp} are colored bluish and reddish, respectively. The shift factors range between 10^1 and 10^2.

scattering contrast between the core and the shell of the micelles. This observation is based on the reported behavior at atmospheric pressure of aqueous solutions of PNIPAM and PMMA-*b*-PNIPAM when temperature is increased above T_{cp}.[26,34] The model contains the Guinier-Porod term (eqs S14−S17 in the SI), which gives insights into the average size R_g and the surface structure of the aggregates, and the Ornstein−Zernike structure factor. The presence of the Ornstein−Zernike term indicates that the aggregates feature concentration fluctuations, implying that they still contain a certain amount of D_2O. This may be attributed to the presence of small water pockets or to a variable water content in the PNIPAM chains around the PMMA cores.

Finally, the SANS curves measured in the two-phase region at 35 and 75 MPa were modeled by eq 3 (Figure 4c). The same contributions as in eq 1 are used, i.e., the Porod term for the scattering from large aggregates, the form and structure factors for the scattering of single micelles, the Ornstein−Zernike structure factor which describes the concentration fluctuations inside the shell of the micelles, and a constant background. However, now the form factor of spherical core−shell micelles with a constant SLD in the shell (eqs S18 and S19 in the SI) and the hard-spheres structure factor are used, in consistency with our previous work.[34] Considering that the SLD in the shell depends on the degree of hydration of the micellar shell, the phase transition from the one-phase to the two-phase region implies a redistribution of the water inside the micellar shell.

3.2.3. Structural Parameters from the Temperature Scans. In this section, the most relevant structural parameters are presented and discussed. Specifically, we show the micellar core radius R_c, the micellar radius R_m, the hard-sphere radius R_{HS}, the volume fraction of the correlated micelles, f_s, and the solvent fraction Φ in the micellar shell, the latter in the two-phase region. The other structural parameters, such as the correlation length ξ, the second virial coefficient b_2, the decay length of the SLD in the shell, α, and the Porod exponent m are shown and discussed in Section 4 of the SI. Others, such as the scaling terms of the contributions and the background term, are shown in Tables S1−S7 in the SI.

Figures 5a, b display the values of R_c, R_m, and R_{HS} obtained from fitting the SANS curves for the temperature scans at 0.1 and 75 MPa. Below the respective T_{cp}, R_c exhibits values of ca. 4 nm for both pressures, independent of temperature, indicating that the core size is not affected by a change of temperature or pressure in the one-phase region. The value of

https://doi.org/10.1021/acs.macromol.4c01591
Macromolecules 2024, 57, 10263−10274

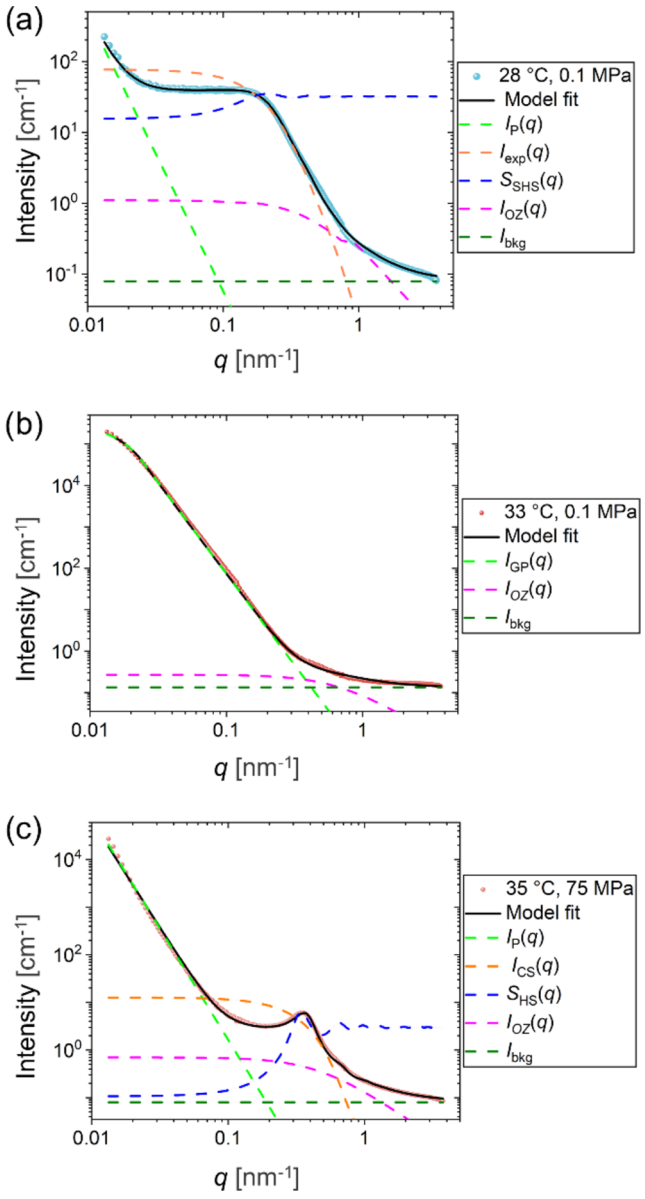

Figure 4. Representative SANS curves from the PMMA-*b*-PNIPAM solution (symbols) with the model fits at (a) 28 °C and 0.1 MPa; (b) 33 °C and 0.1 MPa; and (c) 35 °C and 75 MPa. Solid black lines: overall model fit; dashed lines: individual contributions of the model fits, as given in the legends.

R_c is lower than the contour length of 5.3 nm,[34] as expected, but larger than the end-to-end to distance for an ideal chain conformation (R_c = 2.1 nm). Possibly, the inner part of the PNIPAM shell contributes to R_c. PMMA and dehydrated PNIPAM cannot be distinguished easily, since their SLDs are similar: 1.06×10^{-4} nm^{-2} (PMMA) and 0.814×10^{-4} nm^{-2} (PNIPAM). In fact, the SLD of PNIPAM with a volume fraction of D_2O of 4% matches the SLD of PMMA. We conclude that the micellar core consists of PMMA and strongly dehydrated PNIPAM. It is worth noticing that these values of R_c are larger than those determined previously by SAXS, which range between 2.5 and 3.0 nm.[34] We attribute this difference to the higher contrast between PMMA and dry PNIPAM in X-ray scattering (the X-ray SLDs of PMMA and dry PNIPAM are 10.82×10^{-4} and 10.30×10^{-4} nm^{-2}, respectively). This allows to distinguish between the two blocks even when the micellar shell is partially dehydrated.

At 0.1 MPa, the micellar radius R_m decreases from ca. 15.9 nm to ca. 13.5 nm as temperature is increased to 29 °C, and then increases to ca. 15.1 nm at 30 °C (Figure 5a). Since R_c remains constant, the change of R_m is caused mostly by a change of the shell thickness ΔR. The increase of R_m just below T_{cp} at atmospheric pressure was reported previously for PS-*b*-PNIPAM in D_2O.[38] It was attributed to the partial release of water from the inner region of the micellar shell, which triggers the formation of hydrogen bonds between neighboring PNIPAM segments, causing them to acquire a more stretched conformation. At 75 MPa (Figure 5b), R_m decreases progressively from ca. 14.9 nm to ca. 13.0 nm as temperature is raised until T_{cp}. Similar findings are made at 35 MPa.

At 0.1 MPa and below T_{cp}, the hard-sphere radius R_{HS} has values similar or slightly larger to the ones of R_m (Figure 5a). Thus, the micelles do not interpenetrate. In contrast, at 35 and 75 MPa, R_{HS} is slightly smaller than R_m between 28 °C and T_{cp} (Figures 5b and S3a in the SI). This indicates that the application of pressure enhances the attractive interaction between the correlated micelles in the one-phase region, resulting in a stronger interpenetration.

We cannot obtain structural information about the single micelles above T_{cp} in the temperature scan at 0.1 MPa due to the loss of scattering contrast between the micellar core and shell. The radius of gyration R_g of the aggregates is determined in this temperature range. R_g increases from ca. 25 to ca. 145 nm as temperature is increased up to 35 °C (inset of Figure 5a). Since the loss of scattering contrast between the micellar core and shell remains at 35 °C, indicating that rehydration of the micellar shell and intermicellar regions does not occur, we can assume that the growth of the aggregates is mostly caused by the aggregation of small clusters of collapsed micelles, and not by their rehydration. For the temperature scans at 35 and 75 MPa, R_g cannot be determined because the Guinier region of the scattering of the aggregates does not resolve within the available q-range. Accordingly, R_g is larger in the two-phase regions at 35 and 75 MPa. We attribute the smaller size of the aggregates at atmospheric pressure to the glassy nature of the PNIPAM shell (T_g of dry PNIPAM = 133−134 °C[34,70]) when it strongly dehydrates, which restricts the mobility of the chains forming the micellar shell, preventing the aggregates from growing further. At high pressure, on the other hand, the higher hydration of the aggregates is related to a more swollen conformation of the PNIPAM shell blocks inside the aggregates. Our present q-range does not allow us to determine the aggregate size; however, previous studies on an aqueous solution of PNIPAM homopolymers showed that an increase in pressure leads to the formation of larger mesoglobules in the two-phase region due to their higher water content.[26]

At 75 MPa, R_c remains constant at ca. 4 nm upon crossing the coexistence line (Figure 5b). Thus, when pressure is applied, the change in the solubility of the PNIPAM shell does not influence the size of the micellar core. Also, R_{HS} decreases compared to R_m above T_{cp}, indicating that the degree of interpenetration between the micelles increases.

Figure 5c,d show the volume fraction of the correlated micelles f_s at 0.1 and 75 MPa. At 0.1 MPa (Figure 5c), f_s decreases from ca. 0.19 to ca. 0.05 as temperature is increased up to T_{cp}. Thus, the aggregates of micelles tend to dissociate as the temperature approaches T_{cp}. The existence of these aggregates may explain the presence of the straight decay

https://doi.org/10.1021/acs.macromol.4c01591
Macromolecules 2024, 57, 10263−10274

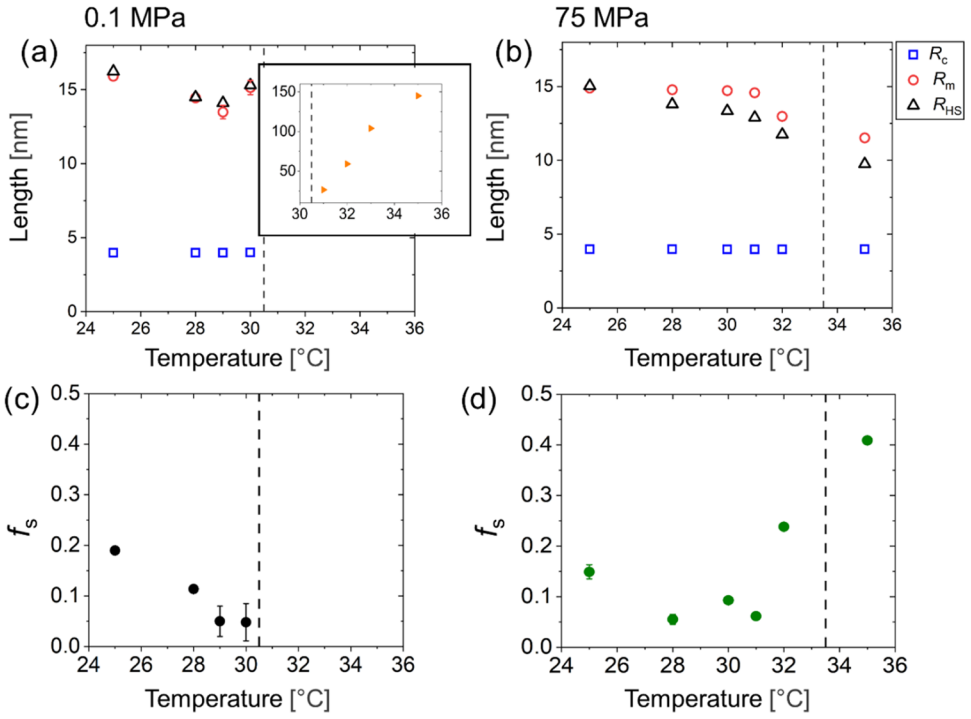

Figure 5. Structural parameters from the model fits of the SANS data from the temperature scans at 0.1 MPa (left panel) and 75 MPa (right panel). (a, b) Core radius R_c (blue open squares), micellar radius R_m (red open spheres), hard-sphere radius R_{HS} (black open up triangles), and radius of gyration of the aggregates, R_g (orange open right triangles), inset in (a). (c, d) Volume fraction of the correlated micelles f_s. In all graphs, the black dashed vertical lines indicate T_{cp} determined from the SANS measurements.

observed at low q-values, as seen in Figure 3a. Further, the micelles forming these aggregates do not interpenetrate as discussed above regarding the values of R_m and R_{HS}. At 75 MPa (Figure 5d), a different scenario is observed below T_{cp}: f_s exhibits an initial decrease below 28 °C from ca. 0.15 to ca. 0.06, and remains below 0.1, as the temperature is raised further up to 32 °C; however, at 33 °C, f_s features a marked increase to ca. 0.24. This nonmonotonous behavior of fs below T_{cp} is also found at 35 MPa (Figure S3b in the SI). Thus, the stronger hydration of the micellar shell induced by applying pressure, has a significant effect on the aggregation behavior of the micelles, which leads to a nonmonotonous behavior of f_s below T_{cp}. Above T_{cp}, f_s increases substantially to ca. 0.21 and ca. 0.41 at 35 and 75 MPa, respectively (Figures 5d and S3b in the SI). This indicates that pressure increases the spatial correlation of the micelles that form the aggregates in the two-phase region. This is evident from the sharpness of the correlation peaks in the two-phase region (red curves in Figures 3b and S2 in the SI).

Table 1 shows the solvent fraction Φ in the micellar shell in the two-phase region. At 35 °C, namely after crossing the coexistence line in the temperature scans, we obtain that Φ = 0.80 and Φ = 0.85 at 35 and 75 MPa, respectively. The higher hydration of the micellar shell at 75 MPa is in consistency with the larger shell thickness at 75 MPa ($\Delta R \cong 4.5$ nm) than at 35 MPa ($\Delta R \cong 3.6$ nm). These results agree with previous molecular dynamics (MD) simulations performed on PNIPAM homopolymers, which show that the isothermal rise of pressure conducted above T_{cp} induces a size increase of PNIPAM due to the higher amount of hydration water in contact with the polymer.[28]

Table 1. Solvent Volume Fraction in the Micellar Shell for the PMMA-*b*-PNIPAM Solution in the Two-Phase Region

T [°C]	p [MPa]	Φ
35.0	35	0.80 ± 0.01
35.0	75	0.85 ± 0.01
31.8	85	0.79 ± 0.02
31.8	90	0.84 ± 0.01
31.8	100	0.89 ± 0.01

3.2.4. Isothermal Pressure Scan. Figure 6 depicts the SANS curves from the pressure scan conducted at 31.8 °C across the coexistence line. In the one-phase region, they show remarkable similarity to the curves at 31 and 32 °C from the temperature scan at 75 MPa. The curve at 50 MPa shows a weak shoulder at $q \cong 0.3$ nm^{-1}, which becomes a prominent correlation peak as pressure is increased across the coexistence line. In the one phase region, a decay is present in the q-range between 0.03 and 0.2 nm^{-1}, whose intensity decreases with pressure. Also, at low q-values ($q < 0.03$ nm^{-1}), we observe a second decay. This second decay is observed at higher q-values as pressure is increased across the coexistence line. In the two-phase region, the curves feature a strong correlation peak at $q \cong 0.3$ nm^{-1}. The position of the correlation peaks does not shift noticeably as pressure is increased, suggesting that the average distance between the correlated micelles is not affected by an isothermal increase of pressure.

Figure 7a shows the structural parameters obtained from the form and structure factor by fitting the SANS curves, namely, R_c, R_m, and R_{HS}. R_c remains constant at ca. 4 nm at both sides of the coexistence line. Accordingly, isothermal pressure changes do not significantly alter the dimensions of the micellar core. R_m decreases slightly (ca. 0.3 nm) as pressure is increased within the one-phase region. However, this change is within the uncertainties of the fits. Thus, we cannot

https://doi.org/10.1021/acs.macromol.4c01591
Macromolecules 2024, 57, 10263−10274

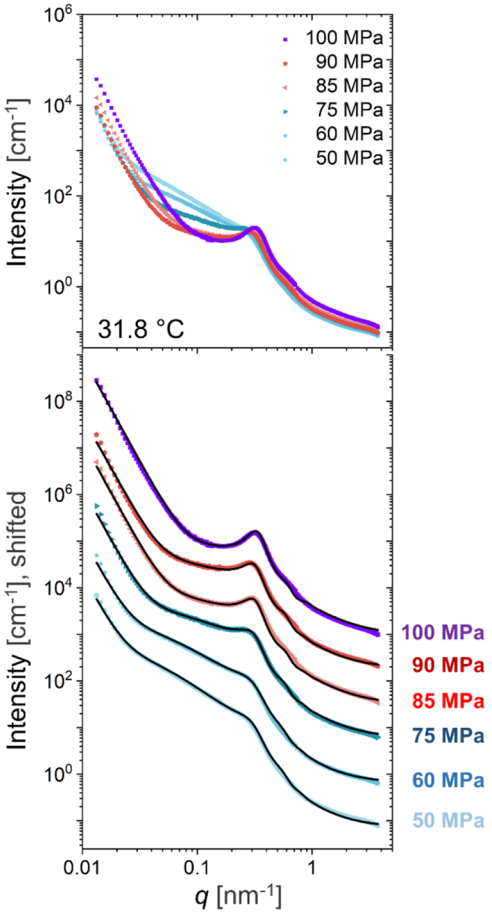

Figure 6. SANS data of the PMMA-*b*-PNIPAM solution (50 g L^{-1} in D_2O) from the pressure scan at 31.8 °C. Upper graphs: unshifted data, lower graphs: vertically shifted data (symbols) with model fits (solid black lines). The SANS curves in the one- and two-phase region are colored bluish and reddish, respectively. The shift factors range between 10^1 and 10^2.

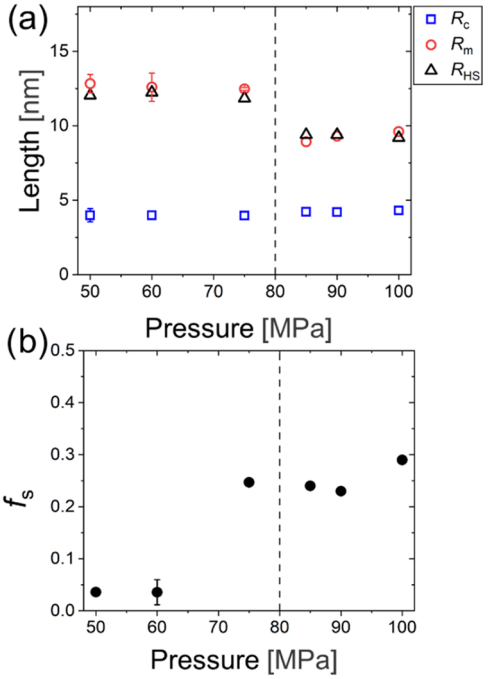

Figure 7. (a) Structural parameters from the model fits to the SANS data for the pressure scan at 31.8 °C. Core radius R_c (blue open squares), micellar radius R_m (red open spheres), and hard-sphere radius R_{HS} (black open up triangles). (b) Volume fraction of the correlated micelles, f_s. In all graphs, the black dashed vertical lines indicate the position of the coexistence line determined from the SANS measurements.

unequivocally assign a change of R_m in this region. After crossing the coexistence line, R_m increases slightly as pressure is raised up to 100 MPa. Also, over the entire pressure range, R_m and R_{HS} exhibit roughly the same values. Thus, the correlated micelles do not interpenetrate significantly. This differs from the behavior in the temperature scans at 35 and 75 MPa, in which the degree of interpenetration between the correlated micelles increases as the temperature is raised across T_{cp}.

The pressure dependence of the volume fraction of correlated micelles f_s is displayed in Figure 7b. f_s remains at ca. 0.04 for pressures lower than 60 MPa. f_s increases considerably to ca. 0.25 when pressure is raised to 75 MPa, and increases further to ca. 0.29 at 100 MPa. This behavior is similar to the one observed in the temperature scan at 75 MPa (Figure 5d), in which the marked increase of f_s occurs below T_{cp} (T = 32 °C). Hence, the aggregation of the micelles begins in the one-phase region as the coexistence line is approached. This indicates that, when pressure is applied, the phase transition occurs in a broader pressure or temperature range across the coexistence line. The aforementioned is in accordance with the behavior observed by turbidimetry (Section 3.1): The transmission decay at the cloud point becomes broader as the pressure increases.

The solvent fraction inside the micellar shell increases from 0.79 to 0.89 when the pressure is raised from 85 to 100 MPa (Table 1), indicating that the micellar shell rehydrates after the redistribution of the solvent within the micellar shell. This occurs after crossing the coexistence line. The micellar shell rehydration explains the increase of R_m observed in Figure 7a, which is mostly provoked by the swelling of the shell thickness of the micelles (see values of ΔR in Table S7 in the SI). This confirms the positive correlation between an isothermal increase of pressure and the hydration of PNIPAM in the two-phase region.

3.2.5. Micellar Structure in Dependence on Temperature and Pressure: Summary of Observations. Based on the analysis of the SANS data in Sections 3.2.2−4, the pressure and temperature dependence of the micellar structure of $PMMA_{21}$-*b*-$PNIPAM_{283}$ in D_2O is depicted schematically in Figure 8. In the one-phase region, weakly correlated spherical core−shell micelles form. The micellar shell is hydrated and exhibits a radially increasing water content. The micellar shell shrinks strongly upon crossing the coexistence line by increasing the temperature at atmospheric pressure. As a consequence, compact aggregates with low water content form in this regime. We infer that the reduction of hydrogen bonds between water and the amide groups of the PNIPAM chains causes the strong dehydration of the micellar shell. Simultaneously, the number of intra- and interchain hydrogen bonds between the secondary amide groups of the PNIPAM chains increases. This observation is consistent with the known behavior of PNIPAM in water under atmospheric pressure.[15] Furthermore, the aggregation of the dehydrated micelles reduces the hydration of the hydrophobic moieties of the PNIPAM chains. Thus, the formation of highly dehydrated

https://doi.org/10.1021/acs.macromol.4c01591
Macromolecules 2024, 57, 10263−10274

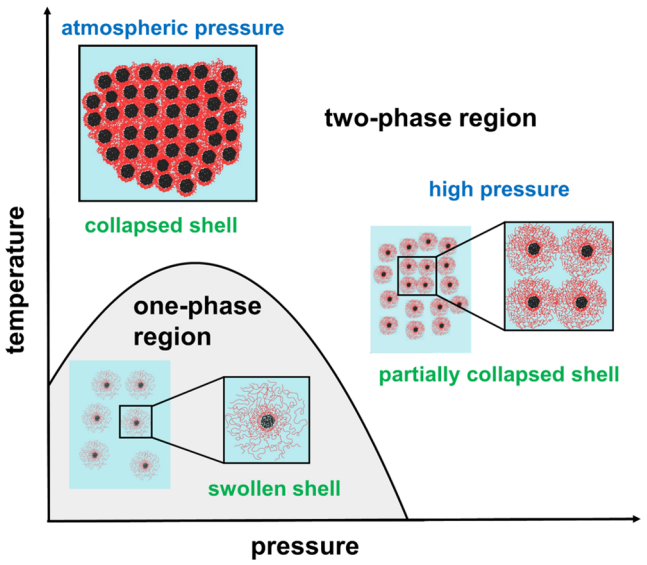

Figure 8. Schematic representation of the structure of the aggregates and the individual micelles in the three regimes indicated in the temperature−pressure frame: one-phase region, two-phase region at atmospheric pressure, and two-phase region at higher pressures. Black: PMMA block; red: PNIPAM block. Images inside a black box are in the same length scale.

aggregates is thermodynamically favorable. Also, we speculate that the formation of hydrogen bonds between the PMMA and PNIPAM blocks does not play an essential role in the collapse of the micellar shell. Differential scanning calorimetry characterization of PMMA-*b*-PNIPAM in the bulk state showed that the two blocks microphase separate.[34,71] Therefore, the immiscibility between the blocks hinders the formation of hydrogen bonds between them. We cannot exclude that the behavior is different when the diblock copolymer forms micelles in aqueous environment; however, we are unaware of any data in this respect.

Large aggregates form upon crossing the coexistence line at high pressures, which consist of highly correlated micelles with a weakly dehydrated shell. This is attributed to a high fraction of polymer−water hydrogen bonds remaining in the two-phase region and the corresponding decrease in the number of PNIPAM−PNIPAM hydrogen bonds, as reported previously for aqueous solutions of PNIPAM.[28,29] The higher hydrophobic hydration of the PNIPAM chains in the two-phase region is entropically unfavorable. However, bulk water changes from an open tetrahedral to a more ordered hexagonal structure when pressure is applied.[72] This would counteract the entropic penalty arising from the hydrophobic hydration, thereby stabilizing the hydrated shell of the micelles forming the aggregates. Also, one may speculate that there is a transition between the two types of aggregates formed by the micelles at low and at high pressure. At present, the nature of this transition is unclear. In the high-pressure regime of the two-phase region, the micellar shell exhibits a homogeneous water content. Furthermore, the water content does not decrease substantially inside the intermicellar region. Moreover, since $R_m < R_{HS}$, the correlated micelles interpenetrate slightly in the one-phase region when pressure is applied. In the two-phase region, the micelles interpenetrate more strongly in the high-pressure temperature scans, while they do not interpenetrate in the pressure scan at 31.8 °C. Thus, the mechanisms by which the micellar interpenetration may occur, such as the formation of interchain hydrogen bonds between the amide groups of PNIPAM chains of different micelles, are enhanced by an isobaric increase in temperature across the coexistence line but not by an isothermal rise in pressure. The micellar core size is not affected by an increase of temperature or pressure, even after crossing the coexistence line, indicating a negligible hydration of the micellar core.

4. CONCLUSIONS

We have studied the effect of pressure on the solubility and the micellar structure of an amphiphilic diblock copolymer consisting of a permanently hydrophobic PMMA block and a thermoresponsive PNIPAM block, extending the current knowledge of the effect of pressure on the structure of PNIPAM homopolymers. The phase diagram of $PMMA_{21}$-*b*-$PNIPAM_{283}$ in D_2O in the temperature−pressure frame was determined by turbidimetry. The maximum of the coexistence line shifts to a lower temperature and pressure compared to aqueous solutions of PNIPAM, indicating the reduction of the water solubility of the PNIPAM chains when copolymerized with short hydrophobic PMMA blocks. SANS revealed the temperature- and pressure-dependence of the micellar structure of $PMMA_{21}$-*b*-$PNIPAM_{283}$ in D_2O. At atmospheric pressure, the micellar shell strongly dehydrates when heated above the cloud point temperature T_{cp} of PNIPAM. Conversely, when pressure is applied, the PNIPAM shell remains hydrated above T_{cp}, leading to a higher shell thickness. The observations above are in line with our previous findings on PNIPAM homopolymers in D_2O, which form aggregates with larger sizes and higher water content when pressure is applied.[26] Therefore, pressure arises as a tool to tune the degree of hydration of the PNIPAM micellar shell when the micelles are heated above the T_{cp} of PNIPAM. Moreover, the PMMA core of the micelles is not significantly altered by temperature and pressure. This last observation differs from the behavior of pEOEOVE-*b*-pHOVE in water when exposed to temperatures between the T_{cp} of pEOEOVE and pHOVE, in which pressure increases the water content of the pEOEOVE micellar core.[50] Consequently, the hydrophobic core of the self-assembled micelles is stable against changes in pressure and temperature when a permanently hydrophobic block is used.

■ ASSOCIATED CONTENT

Supporting Information

The Supporting Information is available free of charge at https://pubs.acs.org/doi/10.1021/acs.macromol.4c01591.

Equations used for modeling the SANS data. Determination of the coexistence line from SANS. SANS data of temperature scan at 35 MPa. Analysis of the additional structural parameters from model fits of SANS data. Fitting parameters from model fits of SANS data (PDF)

■ AUTHOR INFORMATION

Corresponding Authors

Alfons Schulte − *Department of Physics and College of Optics and Photonics, University of Central Florida, Orlando, Florida 32816, United States;* orcid.org/0000-0003-0824-8572; Email: Alfons.schulte@ucf.edu

Christine M. Papadakis − *TUM School of Natural Sciences, Physics Department, Soft Matter Physics Group, Technical University of Munich, 85748 Garching, Germany;*

https://doi.org/10.1021/acs.macromol.4c01591
Macromolecules 2024, 57, 10263−10274

orcid.org/0000-0002-7098-3458; Email: papadakis@tum.de

Authors

Pablo A. Alvarez Herrera − *TUM School of Natural Sciences, Physics Department, Soft Matter Physics Group, Technical University of Munich, 85748 Garching, Germany;* orcid.org/0000-0002-5399-0920

Geethu P. Meledam − *TUM School of Natural Sciences, Physics Department, Soft Matter Physics Group, Technical University of Munich, 85748 Garching, Germany;* orcid.org/0000-0003-2167-0428

Bart-Jan Niebuur − *TUM School of Natural Sciences, Physics Department, Soft Matter Physics Group, Technical University of Munich, 85748 Garching, Germany;* Present Address: INM - Leibniz Institute for New Materials, Campus D2 2, 66123 Saarbrücken, Germany

Yamen Taji − *TUM School of Natural Sciences, Physics Department, Soft Matter Physics Group, Technical University of Munich, 85748 Garching, Germany*

Leonardo Chiappisi − *Institut Laue-Langevin, Partnership for Soft Condensed Matter, 38042 Grenoble, France;* orcid.org/0000-0002-4594-2865

Cristiane Henschel − *Universität Potsdam, Institut für Chemie, 14476 Potsdam-Golm, Germany*

André Laschewsky − *Universität Potsdam, Institut für Chemie, 14476 Potsdam-Golm, Germany; Fraunhofer Institute for Applied Polymer Research, 14476 Potsdam-Golm, Germany;* orcid.org/0000-0003-2443-886X

Complete contact information is available at: https://pubs.acs.org/10.1021/acs.macromol.4c01591

Author Contributions

The manuscript was written through contributions of all authors. All authors have given approval to the final version of the manuscript.

Funding

Funding by Deutsche Forschungsgemeinschaft (Pa 771/22−1), the TUM August-Wilhelm Scheer Guest Professor Program and the Faculty Graduate Center Physics of the TUM Physics Department are gratefully acknowledged.

Notes

The authors declare no competing financial interest.

■ ACKNOWLEDGMENTS

We thank Dr. Chia-Hsin Ko and Shu-Hsien Huang (both TUM) for their participation in the beamtime and the Institut Laue-Langevin for beamtime allocation (doi:http://doi.ill.fr/10.5291/ILL-DATA.9-10-1577) and excellent equipment, as well as for the support infrastructure provided within the Partnership for Soft Condensed Matter (PSCM).

■ REFERENCES

(1) Daniel, J. C.; Audebert, R. Small Vol.s and Large Surfaces: The World of Colloids. In *Soft Matter Physics*; Daoud, M.; Williams, C. E., Eds.; Springer-Verlag Berlin Heidelberg GmbH, 1995; pp 87−132.

(2) Porte, G. From Giant Micelles to Fluid Membranes: Polymorphism in Dilute Solutions of Surfactant Molecules. In *Soft Matter Physics*; Daoud, M.; Williams, C. E., Eds.; Springer-Verlag Berlin Heidelberg GmbH, 1995; pp 155−186.

(3) Prost, J.; Williams, C. E. Liquid Crystals: Between Order and Disorder. In *Soft Matter Physics*; Daoud, M.; Williams, C. E., Eds.; Springer-Verlag Berlin Heidelberg GmbH, 1995; pp 289−316.

(4) Jones, R. A. *Soft Condensed Matter*; Oxford University Press, 2002; pp 1−195.

(5) Kleman, M.; Lavrentovich, O. D. *Soft Matter Physics: An Introduction*; Springer, 2003; Vol. *105*−*139*, pp 519−559.

(6) Hamley, I. W. *Introduction to Soft Matter: Synthetic and Biological Self-assembling Materials*; John Wiley & Sons, 2007; pp 1−312.

(7) Aseyev, V.; Tenhu, H.; Winnik, F. M. Non-ionic Thermoresponsive Polymers in Water. In *Self Organized Nanostructures of Amphiphilic Block Copolymers II*; Müller, A. H. E.; Borisov, O., Eds.; Springer: Berlin Heidelberg, 2011; pp 29−89.

(8) Stuart, M. A. C.; Huck, W. T.; Genzer, J.; Müller, M.; Ober, C.; Stamm, M.; Sukhorukov, G. B.; Szleifer, I.; Tsukruk, V. V.; Urban, M.; et al. Emerging Applications of Stimuli-Responsive Polymer Materials. *Nat. Mater.* **2010**, *9* (2), 101−113.

(9) Hu, L.; Zhang, Q.; Li, X.; Serpe, M. J. Stimuli-Responsive Polymers for Sensing and Actuation. *Mater. Horiz.* **2019**, *6* (9), 1774−1793.

(10) Zhao, J.; Lee, V. E.; Liu, R.; Priestley, R. D. Responsive Polymers as Smart Nanomaterials Enable Diverse Applications. *Annu. Rev. Chem. Biomol. Eng.* **2019**, *10*, 361−382.

(11) Doberenz, F.; Zeng, K.; Willems, C.; Zhang, K.; Groth, T. Thermoresponsive Polymers and their Biomedical Application in Tissue Engineering − a Review. *J. Mater. Chem. B* **2020**, *8* (4), 607−628.

(12) Pamies, R.; Zhu, K.; Kjøniksen, A.-L.; Nyström, B. Thermal Response of Low Molecular Weight Poly-(*N*-isopropylacrylamide) Polymers in Aqueous Solution. *Polym. Bull.* **2009**, *62* (4), 487−502.

(13) Halperin, A.; Kröger, M.; Winnik, F. M. Poly(*N*-isopropylacrylamide) Phase Diagrams: Fifty Years of Research. *Angew. Chem., Int. Ed.* **2015**, *54* (51), 15342−15367.

(14) Okada, Y.; Tanaka, F. Cooperative Hydration, Chain Collapse, and Flat LCST Behavior in Aqueous Poly(*N*-isopropylacrylamide) Solutions. *Macromolecules* **2005**, *38* (10), 4465−4471.

(15) Ahmed, Z.; Gooding, E. A.; Pimenov, K. V.; Wang, L.; Asher, S. A. UV Resonance Raman Determination of Molecular Mechanism of Poly(*N*-isopropylacrylamide) Volume Phase Transition. *J. Phys. Chem. B* **2009**, *113* (13), 4248−4256.

(16) Wu, C.; Li, W.; Zhu, X. X. Viscoelastic Effect on the Formation of Mesoglobular Phase in Dilute Solutions. *Macromolecules* **2004**, *37* (13), 4989−4992.

(17) Aseyev, V.; Hietala, S.; Laukkanen, A.; Nuopponen, M.; Confortini, O.; Du Prez, F. E.; Tenhu, H. Mesoglobules of thermoresponsive Polymers in Dilute Aqueous Solutions Above the LCST. *Polymer* **2005**, *46* (18), 7118−7131.

(18) Kujawa, P.; Aseyev, V.; Tenhu, H.; Winnik, F. M. Temperature-Sensitive Properties of Poly(*N*-isopropylacrylamide) Mesoglobules Formed in Dilute Aqueous Solutions Heated above Their Demixing Point. *Macromolecules* **2006**, *39* (22), 7686−7693.

(19) Balu, C.; Delsanti, M.; Guenoun, P.; Monti, F.; Cloitre, M. Colloidal Phase Separation of Concentrated PNIPAm Solutions. *Langmuir* **2007**, *23* (5), 2404−2407.

(20) Papadakis, C. M.; Niebuur, B.-J.; Schulte, A. Thermoresponsive Polymers under Pressure with a Focus on Poly(*N*-isopropylacrylamide) (PNIPAM). *Langmuir* **2024**, *40* (1), 1−20.

(21) Shibayama, M.; Isono, K.; Okabe, S.; Karino, T.; Nagao, M. SANS Study on Pressure-Induced Phase Separation of Poly(*N*-isopropylacrylamide) Aqueous Solutions and Gels. *Macromolecules* **2004**, *37* (8), 2909−2918.

(22) Ebeling, B.; Eggers, S.; Hendrich, M.; Nitschke, A.; Vana, P. Flipping the Pressure- and Temperature-Dependent Cloud-Point Behavior in the Cononsolvency System of Poly(*N*-isopropylacrylamide) in Water and Ethanol. *Macromolecules* **2014**, *47* (4), 1462−1469.

(23) Niebuur, B.-J.; Chiappisi, L.; Zhang, X.; Jung, F.; Schulte, A.; Papadakis, C. M. Formation and Growth of Mesoglobules in Aqueous Poly(*N*-isopropylacrylamide) Solutions Revealed with Kinetic Small-Angle Neutron Scattering and Fast Pressure Jumps. *ACS Macro Lett.* **2018**, *7* (10), 1155−1160.

(24) Niebuur, B.-J.; Deyerling, A.; Höfer, N.; Schulte, A.; Papadakis, C. M. Cononsolvency of the Responsive Polymer poly(*N*-isopropylacrylamide) in Water/Methanol Mixtures: a Dynamic Light Scattering Study of the Effect of Pressure on the Collective Dynamics. *Colloid Polym. Sci.* **2022**, *300*, 1269−1279.
(25) Osaka, N.; Shibayama, M.; Kikuchi, T.; Yamamuro, O. Quasi-Elastic Neutron Scattering Study on Water and Polymer Dynamics in Thermo/Pressure Sensitive Polymer Solutions. *J. Phys. Chem. B* **2009**, *113* (39), 12870−12876.
(26) Niebuur, B.-J.; Claude, K.-L.; Pinzek, S.; Cariker, C.; Raftopoulos, K. N.; Pipich, V.; Appavou, M.-S.; Schulte, A.; Papadakis, C. M. Pressure-Dependence of Poly(*N*-isopropylacrylamide) Mesoglobule Formation in Aqueous Solution. *ACS Macro Lett.* **2017**, *6* (11), 1180−1185.
(27) Niebuur, B.-J.; Lohstroh, W.; Appavou, M.-S.; Schulte, A.; Papadakis, C. M. Water Dynamics in a Concentrated Poly(*N*-isopropylacrylamide) Solution at Variable Pressure. *Macromolecules* **2019**, *52* (5), 1942−1954.
(28) Tavagnacco, L.; Chiessi, E.; Zaccarelli, E. Molecular Insights on Poly(*N*-isopropylacrylamide) Coil-to-Globule Transition Induced by Pressure. *Phys. Chem. Chem. Phys.* **2021**, *23* (10), 5984−5991.
(29) Meersman, F.; Wang, J.; Wu, Y.; Heremans, K. Pressure Effect on the Hydration Properties of Poly(*N*-isopropylacrylamide) in Aqueous Solution Studied by FTIR Spectroscopy. *Macromolecules* **2005**, *38* (21), 8923−8928.
(30) Srinivas, G.; Discher, D. E.; Klein, M. L. Self-assembly and Properties of Diblock Copolymers by Coarse-grain Molecular Dynamics. *Nat. Mater.* **2004**, *3* (9), 638−644.
(31) Blanazs, A.; Armes, S. P.; Ryan, A. J. Self-assembled Block Copolymer Aggregates: From Micelles to Vesicles and Their Biological Applications. *Macromol. Rapid Commun.* **2009**, *30* (4−5), 267−277.
(32) Mai, Y.; Eisenberg, A. Self-assembly of Block Copolymers. *Chem. Soc. Rev.* **2012**, *41* (18), 5969−5985.
(33) Zhulina, E. B.; Borisov, O. Theory of Block Polymer Micelles: Recent Advances and Current Challenges. *Macromolecules* **2012**, *45* (11), 4429−4440.
(34) Ko, C.-H.; Henschel, C.; Meledam, G. P.; Schroer, M. A.; Müller-Buschbaum, P.; Laschewsky, A.; Papadakis, C. M. Self-Assembled Micelles from Thermoresponsive Poly(methyl methacrylate)-*b*-poly(*N*-isopropylacrylamide) Diblock Copolymers in Aqueous Solution. *Macromolecules* **2021**, *54* (1), 384−397.
(35) Nuopponen, M.; Ojala, J.; Tenhu, H. Aggregation Behaviour of Well Defined Amphiphilic Diblock Copolymers with Poly(*N*-isopropylacrylamide) and Hydrophobic Blocks. *Polymer* **2004**, *45* (11), 3643−3650.
(36) Zhang, W.; Zhou, X.; Li, H.; Fang, Y.; Zhang, G. Conformational Transition of Tethered Poly(*N*-isopropylacrylamide) Chains in Coronas of Micelles and Vesicles. *Macromolecules* **2005**, *38* (3), 909−914.
(37) Troll, K.; Kulkarni, A.; Wang, W.; Darko, C.; Koumba, A. M. B.; Laschewsky, A.; Müller-Buschbaum, P.; Papadakis, C. M. The Collapse Transition of Poly(styrene-*b*-(*N*-isopropyl acrylamide)) Diblock Copolymers in Aqueous Solution and in Thin Films. *Colloid Polym. Sci.* **2008**, *286* (8−9), 1079−1092.
(38) Adelsberger, J.; Meier-Koll, A.; Bivigou-Koumba, A. M.; Busch, P.; Holderer, O.; Hellweg, T.; Laschewsky, A.; Müller-Buschbaum, P.; Papadakis, C. M. The Collapse Transition and the Segmental Dynamics in Concentrated Micellar Solutions of P(S-*b*-NIPAM) Diblock Copolymers. *Colloid Polym. Sci.* **2011**, *289* (5−6), 711−720.
(39) Laschewsky, A.; Müller-Buschbaum, P.; Papadakis, C. M. *Thermo-responsive Amphiphilic Di- and Triblock Copolymers Based on Poly(N-isopropylacrylamide) and Poly(methoxy diethylene glycol acrylate): Aggregation and Hydrogel Formation in Bulk Solution and in Thin Films*; Springer International Publishing: Cham, 2013; pp 15−34.
(40) Cao, M.; Nie, H.; Hou, Y.; Han, G.; Zhang, W. Synthesis of Star Thermoresponsive Amphiphilic Block Copolymer Nano-assemblies and the Effect of Topology on their Thermoresponse. *Polym. Chem.* **2019**, *10* (3), 403−411.
(41) Ko, C.-H.; Henschel, C.; Meledam, G. P.; Schroer, M. A.; Guo, R.; Gaetani, L.; Müller-Buschbaum, P.; Laschewsky, A.; Papadakis, C. M. Co-Nonsolvency Effect in Solutions of Poly(methyl methacrylate)-*b*-poly(*N*-isopropylacrylamide) Diblock Copolymers in Water/Methanol Mixtures. *Macromolecules* **2021**, *54* (12), 5825−5837.
(42) Hamley, I. W.; Castelletto, V. Small-angle Scattering of Block Copolymers: in the Melt, Solution and Crystal States. *Prog. Polym. Sci.* **2004**, *29* (9), 909−948.
(43) Liu, Y.; Spring, J. D.; Steinhart, M.; Bansil, R. Pressure Jump Kinetics of Disorder to BCC Ordering in Diblock Copolymer Micelles in a Selective Solvent. *Macromolecules* **2012**, *45* (22), 9147−9154.
(44) Cheng, G.; Hammouda, B.; Perahia, D. Polystyrene-*block*-Polyisoprene Diblock-Copolymer Micelles: Coupled Pressure and Temperature Effects. *Macromol. Chem. Phys.* **2014**, *215* (8), 776−782.
(45) Castelletto, V.; Newby, G.; Hamley, I.; Noirez, L.; Baroni, P. Pressure Effects Revealed by Small Angle Neutron Scattering on Block Copolymer Gels. *Langmuir* **2008**, *24* (15), 8319−8324.
(46) Clover, B.; Hammouda, B. SANS from P85/Water-*d* under Pressure. *Langmuir* **2010**, *26* (9), 6625−6629.
(47) Winoto, W.; Adidharma, H.; Shen, Y.; Radosz, M. Micellization Temperature and Pressure for Polystyrene-*block*-polyisoprene in Subcritical and Supercritical Propane. *Macromolecules* **2006**, *39* (23), 8140−8144.
(48) Osaka, N.; Okabe, S.; Karino, T.; Hirabaru, Y.; Aoshima, S.; Shibayama, M. Micro- and Macrophase Separations of Hydrophobically Solvated Block Copolymer Aqueous Solutions Induced by Pressure and Temperature. *Macromolecules* **2006**, *39* (17), 5875−5884.
(49) Osaka, N.; Shibayama, M. Pressure-Induced Phase Transitions of Hydrophobically Solvated Block-Copolymer Solutions. *Phys. Rev. Lett.* **2006**, *96* (4), No. 048303.
(50) Osaka, N.; Miyazaki, S.; Okabe, S.; Endo, H.; Sasai, A.; Seno, K.; Aoshima, S.; Shibayama, M. Pressure-Induced Reentrant Micellization of Amphiphilic Block Copolymers in Dilute Aqueous Solutions. *J. Chem. Phys.* **2007**, *127* (9), No. 094905.
(51) Lindner, P.; May, R. P.; Timmins, P. A. Upgrading of the SANS instrument D11 at the ILL. *Phys. B: Condens. Matter* **1992**, *180*−*181*, 967−972.
(52) Liquid Pressure Cell 21PL30AO2 2023 https://www.ill.eu/users/support-labs-infrastructure/sample-environment/equipment/high-pressures/liquid-pressure-cells/liquid-pressure-cell-21pl30ao2. (accessed July 7, 2023).
(53) Richard, D.; Ferrand, M.; Kearley, G. J. Analysis and Visualisation of Neutron-Scattering Data. *J. Neutron Res.* **1996**, *4*, 33−39.
(54) Porod, G. Die Röntgenkleinwinkelstreuung von dichtgepackten kolloiden Systemen. *Kolloid-Z.* **1951**, *124* (2), 83−114.
(55) Kohlbrecher, J. *User Guide for the SASfit Software Package*; Paul Scherrer Institute. Laboratory for Neutron Scattering (LNS), 2018.
(56) Baxter, R. J. Percus−Yevick Equation for Hard Spheres with Surface Adhesion. *J. Chem. Phys.* **1968**, *49* (6), 2770−2774.
(57) Menon, S. V. G.; Kelkar, V. K.; Manohar, C. Application of Baxter's Model to the Theory of Cloud Points of Nonionic Surfactant Solutions. *Phys. Rev. A* **1991**, *43* (2), No. 1130.
(58) Shibayama, M.; Tanaka, T.; Han, C. C. Small Angle Neutron Scattering Study on Poly(*N*-isopropyl acrylamide) Gels Near Their Volume-Phase Transition Temperature. *J. Chem. Phys.* **1992**, *97* (9), 6829−6841.
(59) Koberstein, J. T.; Morra, B.; Stein, R. S. The Determination of Diffuse-Boundary Thicknesses of Polymers by Small-Angle X-ray Scattering. *J. Appl. Crystallogr.* **1980**, *13* (1), 34−45.
(60) Hammouda, B. A New Guinier-Porod Model. *J. Appl. Crystallogr.* **2010**, *43* (4), 716−719.
(61) Schulz, G. V. Über die Kinetik der Kettenpolymerisationen. V. *Z. Phys. Chem.* **1939**, *43B* (1), 25−46.
(62) Möller, J.; Grobelny, S.; Schulze, J.; Bieder, S.; Steffen, A.; Erlkamp, M.; Paulus, M.; Tolan, M.; Winter, R. Reentrant Liquid-

Liquid Phase Separation in Protein Solutions at Elevated Hydrostatic Pressures. *Phys. Rev. Lett.* **2014**, *112* (2), No. 028101.
(63) Bartlett, P.; Ottewill, R. H. A Neutron Scattering Study of the Structure of a Bimodal Colloidal Crystal. *J. Chem. Phys.* **1992**, *96* (4), 3306−3318.
(64) Percus, J. K.; Yevick, G. J. Analysis of Classical Statistical Mechanics by Means of Collective Coordinates. *Phys. Rev.* **1958**, *110* (1), No. 1.
(65) Kohlbrecher, J.; Bressler, I. Updates in SASfit for Fitting Analytical Expressions and Numerical Models to Small-Angle Scattering Patterns. *J. Appl. Crystallogr.* **2022**, *55* (6), 1677−1688.
(66) Kyriakos, K.; Aravopoulou, D.; Augsbach, L.; Sapper, J.; Ottinger, S.; Psylla, C.; Rafat, A. A.; Benitez-Montoya, C. A.; Miasnikova, A.; Di, Z.; Laschewsky, A.; Müller-Buschbaum, P.; Kyritsis, A.; Papadakis, C. M. Novel Thermoresponsive Block Copolymers Having Different Architectures—Structural, Rheological, Thermal, and Dielectric Investigations. *Colloid Polym. Sci.* **2014**, *292* (8), 1757−1774.
(67) Kyriakos, K.; Philipp, M.; Adelsberger, J.; Jaksch, S.; Berezkin, A. V.; Lugo, D. M.; Richtering, W.; Grillo, I.; Miasnikova, A.; Laschewsky, A.; Müller-Buschbaum, P.; Papadakis, C. M. Cononsolvency of Water/Methanol Mixtures for PNIPAM and PS-*b*-PNIPAM: Pathway of Aggregate Formation Investigated Using Time-Resolved SANS. *Macromolecules* **2014**, *47* (19), 6867−6879.
(68) Adelsberger, J.; Kulkarni, A.; Jain, A.; Wang, W.; Bivigou-Koumba, A. M.; Busch, P.; Pipich, V.; Holderer, O.; Hellweg, T.; Laschewsky, A.; Müller-Buschbaum, P.; Papadakis, C. M. Thermoresponsive PS-*b*-PNIPAM-*b*-PS Micelles: Aggregation Behavior, Segmental Dynamics, and Thermal Response. *Macromolecules* **2010**, *43* (5), 2490−2501.
(69) Jain, A.; Kulkarni, A.; Koumba, A. B.; Wang, W.; Busch, P.; Laschewsky, A.; Müller-Buschbaum, P.; Papadakis, C. M. Micellar Solutions of a Symmetrical Amphiphilic ABA Triblock Copolymer with a Temperature-Responsive Shell. *Macromol. Symp.* **2010**, *291*−*292*, 221−229.
(70) Nuopponen, M.; Kalliomäki, K.; Laukkanen, A.; Hietala, S.; Tenhu, H. A−B−A Stereoblock Copolymers of N-isopropylacrylamide. *J. Polym. Sci., Part A: Polym. Chem.* **2008**, *46* (1), 38−46.
(71) Li, J.-J.; Zhou, Y.-N.; Luo, Z.-H. Thermal-responsive Block Copolymers for Surface with Reversible Switchable Wettability. *Ind. Eng. Chem. Res.* **2014**, *53* (47), 18112−18120.
(72) Grigera, J. R.; McCarthy, A. N. The Behavior of the Hydrophobic Effect under Pressure and Protein Denaturation. *Biophys. J.* **2010**, *98* (8), 1626−1631.

https://doi.org/10.1021/acs.macromol.4c01591
Macromolecules 2024, 57, 10263−10274